

1 **Projecting circum-Arctic excess ground ice melt with a sub-grid representation in the Community**  
2 **Land Model**

3 Lei Cai<sup>1</sup>, Hanna Lee<sup>1</sup>, Kjetil Schanke Aas<sup>2</sup>, Sebastian Westermann<sup>2</sup>

4 <sup>1</sup>NORCE Norwegian Research Centre, Bjerknes Centre for Climate Research, 5008, Bergen, Norway

5 <sup>2</sup>Department of Geosciences, University of Oslo, Oslo, 0315, Norway

6 *Correspondence to:* Lei Cai (leca@norce.no)

7 **Abstract** To address the longstanding underrepresentation of the influences of highly variable ground  
8 ice content on the trajectory of permafrost conditions simulated in Earth System Models under a warming  
9 climate, we implement a sub-grid representation of excess ground ice within permafrost soils using the  
10 latest version of the Community Land Model (CLM5). Based on the original CLM5 tiling hierarchy, we  
11 duplicate the natural vegetated landunit by building extra tiles for up to three cryostratigraphies with  
12 different amounts of excess ice for each grid cell. For the same total amount of excess ice, introducing  
13 sub-grid variability in excess ice contents leads to different excess ice melting rates at the grid level. In  
14 addition, there are impacts on permafrost thermal properties and local hydrology with sub-grid  
15 representation. We evaluate this new development with single-point simulations at the Lena river delta,  
16 Siberia, where three sub-regions with distinctively different excess ice conditions are observed. A triple-  
17 landunit case accounting for this spatial variability conforms well to previous model studies for the Lena  
18 river delta and displays a markedly different dynamics of future excess ice thaw compared to a single-  
19 landunit case initialized with average excess ice contents. For global simulations, we prescribed a tiling  
20 scheme combined with our sub-grid representation to the global permafrost region using presently  
21 available circum-Arctic ground ice data. The sub-grid scale excess ice produces significant melting of  
22 excess ice under a warming climate and enhances the representation of sub-grid variability of surface  
23 subsidence on a global scale. Our model development makes it possible to portray more details on the  
24 permafrost degradation trajectory depending on the sub-grid soil thermal regime and excess ice melting,  
25 which also shows a strong indication that accounting for excess ice is a prerequisite of a reasonable  
26 projection of permafrost thaw. The modeled permafrost degradation with sub-grid excess ice follows the  
27 pathway that continuous permafrost transforms into discontinuous permafrost before it disappears,  
28 including surface subsidence and talik formation, which are highly permafrost-relevant landscape  
29 changes excluded from most land models. Our development of sub-grid representation of excess ice  
30 demonstrates a way forward to improve the realism of excess ice melt in global land models, but further  
31 developments require substantially improved global observational datasets on both the horizontal and  
32 vertical distributions of excess ground ice.

33 **1. Introduction**

34 Permafrost soils are often characterized by different types of ground ice that can exceed the pore  
35 space (Brown et al. 1997; Zhang et al., 1999). The presence of such “excess” ground ice can alter the

36 permafrost thermal regime and landscape structure. Widespread thawing of permafrost is expected in a  
37 warmer future climate and modeling studies suggest large-scale degradation of near-surface permafrost  
38 at the end of the 21st century (Lawrence et al., 2008 & 2011). Melting of ground ice due to active layer  
39 thickening releases water in the form of surface runoff, subsurface flow, or both, causing surface  
40 subsidence and modifying the local hydrological cycle (West and Plug, 2008; Grosse et al., 2011; Kokelj  
41 et al., 2013; Westermann et al., 2016). In addition to containing ground ice, some permafrost soils store  
42 massive amounts of carbon, which could be released to the atmosphere in the form of greenhouse gases  
43 upon thawing (Walter et al., 2006; Zimov et al., 2006; Schuur et al., 2008), possibly making a positive  
44 feedback to amplify future climate change (Koven et al., 2011; Schaefer et al., 2014; Burke et al., 2013).  
45 The existence of excess ice and its distribution in permafrost can significantly affect the rate of permafrost  
46 thawing (Westermann et al., 2016; Nitzbon et al., 2020), and in turn, the rate of soil carbon release  
47 (Hugelius et al., 2014; Schuur et al., 2015; Turetsky et al., 2019). Therefore, better projections of excess  
48 ice melt are critical to improve our understanding of the impacts of permafrost thaw on corresponding  
49 climatic impacts.

50 Previous studies address excess ice modeling on the local or regional scale, in which the small study  
51 area makes it possible for detailed configurations of the cryostratigraphy of permafrost and excess ice  
52 based on observations. Simulations for the Lena river delta have retrieved the permafrost thermal  
53 dynamics fairly close to the observations with excess ice incorporated in the modeling (Westermann et  
54 al., 2016). A two-tile approach allowing lateral heat exchange between two land elements demonstrated  
55 that maintaining thermokarst ponds requires the heat loss from water to the surrounding land (Langer et  
56 al., 2016). A similar tiling approach has been applied to projecting the landscape changes due to  
57 permafrost thaw for ice-wedge polygons and peat plateaus with different features of ice melting and  
58 surface subsidence (Aas et al., 2019; Nitzbon et al., 2019).

59 On the global scale, the land components of Earth System Models (ESMs) have significant  
60 capabilities of representing key permafrost physics. In the Community Land Model (CLM), for example,  
61 the representation of permafrost-associated processes has been continuously improved. By including key  
62 thermal and hydrological processes of permafrost, the CLM version 4 (CLM4) has reasonably  
63 reproduced the global distribution of permafrost (Lawrence et al., 2008; Lawrence et al., 2012; Slater  
64 and Lawrence, 2013). Projections based on the CLM4 under its highest warming scenario (RCP8.5) have  
65 shown over 50% degradation of near-surface permafrost by 2100 (Lawrence et al., 2012). Moreover, the  
66 recently released CLM5 has more advanced representations of many biogeophysical and biogeochemical  
67 processes (Lawrence et al., 2019). A refined soil profile and upgraded snow accumulation and  
68 densification scheme in the CLM5 could contribute to simulating more realistic permafrost thermal  
69 regimes, whereas upgrades on biogeochemistry improve simulations of soil carbon release in response  
70 to permafrost thaw. In addition, an excess ice physics scheme has been implemented in CLM4.5  
71 (CLM4.5\_EXICE) by Lee et al. (2014), which allowed for the first-order simulation of surface  
72 subsidence globally by modeling excess ice melt under a warming climate.

73 The homogeneous distribution of excess ice throughout the grid cell in CLM4.5\_EXICE (Lee et al.,  
74 2014) could cause biases in thaw trajectories in the warming climate. In nature, excess ice forms in a  
75 highly localized manner due to a variety of accumulation processes. For instance, segregated ice formed  
76 during frost heave differs substantially in excess ice morphology from ice wedges that are formed from  
77 repeated frost cracking and freezing of penetrating water. Field measurements illustrate that the depth  
78 distribution of ground ice can vary substantially on the order to 10-50 metres horizontally and 0-10 metres  
79 vertically (Pascale et al., 2008; Fritz et al., 2011). The horizontal grid spacing of ESMs, on the other hand,  
80 usually ranges from one to two degrees (~100-200 km horizontal scale), which makes it impossible to  
81 represent localized excess ice. The mismatch in spatial scale between model and the real world raises  
82 concerns for the reliability of excess ice modeling in ESMs. Aside from the homogeneously initialized  
83 excess ice in the grid cell, CLM4.5\_EXICE initializes excess ice in the same soil depths globally (below  
84 1m), regardless of the varying active layer thickness in circum-Arctic permafrost areas (Lee et al., 2014).  
85 Such deficiencies in excess ice parameterization hamper global projections of permafrost thaw including  
86 excess ice with ESMs.

87 To narrow the gap between the high spatial variability of excess ice and the coarse grid spacing in  
88 the ESMs, we applied a sub-grid approach in representing excess ice in permafrost soils within the CLM5  
89 to investigate how presence and melting of excess ice affect land surface physics under a warming climate.  
90 We conducted idealized single-point simulations to examine the robustness of model development, and  
91 furthermore conducted global simulations using a first-order estimate for the spatial distribution of excess  
92 ice and associated cryostratigraphies. Due to the lack of information in global excess ice conditions, it is  
93 not the aim of this study to accurately project excess ice melt and surface subsidence in the 21st century,  
94 but rather to develop and present a functionable process within a land surface model that can eventually  
95 bring permafrost thaw modeling towards a higher degree of accuracy on a global scale. The CLM5 with  
96 sub-grid excess ice representation developed through this study would be ready to serve as a proper  
97 simulation tool on further advancing global excess ice modeling once new datasets become available.

## 98 **2. Methodology**

### 99 **2.1 Sub-grid representation of excess ice in the CLM5**

100 The CLM5 model utilizes a three-level tiling hierarchy to represent sub-grid heterogeneity of  
101 landscapes, which are (from top to bottom) landunits, columns, and patches (Lawrence et al., 2019).  
102 There is only one column (the natural soil column) that is under the natural vegetated landunit, which  
103 represents soil including permafrost. In this study, we modify the CLM5 tiling hierarchy by duplicating  
104 the natural vegetated landunit, making extra landunits for prescribing up to three different excess ice  
105 conditions in permafrost (Figure 1). The original natural vegetated landunit is considered as “natural  
106 vegetated with no excess ice” (hereafter no ice landunit), while we denote the additional landunits as  
107 “natural vegetated with low content of excess ice” (hereafter the low ice landunit), “natural vegetated  
108 with medium content of excess ice” (hereafter the mid ice landunit), and “natural vegetated with high  
109 content of excess ice” (hereafter the high ice landunit). The sub-grid initial conditions of excess ice are

110 imported as part of the surface data, which includes the variables of volumetric excess ice contents,  
111 depths of the top and bottom soil layer of added excess ice, and the area weights of the four landunits.

112 We adopted the excess ice physics from CLM4.5\_EXICE (Lee et al., 2014), including  
113 thermodynamic and hydrological processes. The added excess ice is evenly distributed within each soil  
114 layer. Whereas the original CLM5 model already represents the dynamics of pore ice, our representation  
115 of excess ice physics only addresses the ground ice bodies that exceed soil pore space. The volumetric  
116 excess ice content in this study is defined as the ratio of the volume of excess ice in a soil layer to the  
117 volume of the whole soil layer. For example, a 50% volumetric content of excess ice means the excess  
118 ice body occupies 50% volume of a soil layer, while the rest of soil (and pore ice) occupies the other 50%  
119 volume of the soil layer. If not otherwise notified, the parameter of volumetric ice content in this  
120 manuscript refers only to that of excess ice bodies. After adding excess ice, the soil layer thickness  
121 increases accordingly. Because ice density is considered constant, the increase of soil layer thickness is  
122 linearly proportional to the volumetric content of excess ice. For example, adding an excess ice body  
123 with a 50% volumetric excess ice content doubles the soil layer thickness of the corresponding soil layer.  
124 The revised algorithm for thermal conductivity and heat capacity of soil involves the effects of added  
125 excess ice, while the revised phase change energy equation allows excess ice to melt. The meltwater adds  
126 to soil liquid water in the same soil layer, and it can move to the above layer if the original layer is  
127 saturated. Such numerical implementation replicates how the melt excess ice eventually converts to  
128 runoff and discharges from the soil in case of well-drained conditions. As excess ice melts, soil layer  
129 thickness decreases, which corresponds to surface subsidence due to excess ice melt. In our model  
130 parameterization, excess ice only melts and does not re-form since the applied excess ice physics does  
131 not account for the different ice formation processes.

132 Aside from sub-grid tiles for excess ice, we acknowledge that the version upgrade from CLM4.5 to  
133 CLM5 as the base model modifies the results of excess ice melt compared to the results from Lee et al.  
134 (2014). By default, CLM5 represents soil with a 25-layer profile, for which the top 20 hydrologically  
135 active layers cover 8.5 metres of soil. There are additional 10 soil layers and it is 4.7 metres deeper  
136 compared to the default hydrologically active soil layer profile in CLM4.5, not to mention the  
137 substantially more complex biogeophysical processes (Lawrence et al., 2019). Therefore, we developed  
138 the sub-grid representation of excess ice within the framework of the latest version of CLM. The  
139 duplicated landunits prolong computation time by roughly 10% compared to the original CLM5. We are,  
140 therefore, confident that our model development is highly efficient in addressing the sub-grid excess ice  
141 and subsequent permafrost thaw.

142 We examined the sensitivity of sub-grid excess ice initialization by conducting idealized  
143 experiments (see supplemental material). ~~For overall~~Overall, for the same amount of excess ice in one  
144 grid cell located in the same depth, a higher volumetric excess ice content along with a smaller area  
145 weight results in a later start of excess ice melt and a ~~smaller-lower~~ melting rate. The different melting  
146 features from different sub-grid distributions of excess ice then leads to different hydrological impacts  
147 to the permafrost soil. The ~~results of the~~ idealized experiments ~~in this way verify~~ the necessity of

148 ~~involving-introducing~~ sub-grid configuration of excess ice to the CLM that ~~is-with~~has a typical horizontal  
149 grid spacing of 1-2 degrees. More details are available in the supplemental material.

## 150 **2.2 Single-point simulations for the Lena river delta, Siberia**

151 We conduct single-point simulations for the Lena River delta and compare the CLM5 model results  
152 to reference simulations with the CryoGrid3 model for the same location (Westermann et al., 2016).  
153 Abundant background information is available on the soil and ground ice dynamics from both  
154 observation and modeling, making the Lena river delta a suitable location to further evaluate our model  
155 development. The Lena river delta can be broadly categorized into three different geomorphological units  
156 that have distinctively different subsurface cryostratigraphies of excess ice (Schneider et al., 2009; Ulrich  
157 et al., 2009). In the eastern and central part of the river delta, ground ice has been accumulated in the  
158 comparatively warm Holocene climate. The subsurface sediments (hereafter denoted as “Holocene  
159 ground ice terrain”) are generally super-saturated with wedge ice that can extend up to 9 metres  
160 underground with the volumetric contents of total ground ice (pore ice + excess ice) ranging from 60-  
161 80% (Schwamborn et al., 2002; Langer et al., 2013). On the other hand, higher excess ice contents are  
162 found in Pleistocene sediments in the Lena River Delta (hereafter the “Yedoma Ice complex”), which  
163 are characterized by Yedoma type ground ice (Schirrmeister et al., 2013), which can reach depths of up  
164 to 20-25 metres deep and volumetric contents of total ground ice as high as 90% (Schwamborn et al.,  
165 2002; Schirrmeister et al., 2003 and 2011). Finally, the Northwestern part of the delta features sandy  
166 sediments and is characterized by low excess ice contents (hereafter denoted the “no excess ice terrain”;  
167 Rachold and Grigoriev, 1999; Schwamborn et al., 2002).

168 We determine the area weights of excess ice landunits in one single point based on the spatial pattern  
169 of three subregions (Fedorova et al., 2015). The cryostratigraphy and the volumetric contents of excess  
170 ice strictly follow those in Westermann et al. (2016). Noting that the excess ice initialization scenario in  
171 Westermann et al. (2016) does not necessarily represent the realistic excess ice condition for the Lena  
172 river delta, the purpose of applying the same excess ice cryostratigraphy as in Westermman et al. (2016)  
173 is to evaluate our model development by addressing intercomparisons between model results. Meanwhile,  
174 we did not customize soil properties for different landunits as in Westermann et al. (2016), as our model  
175 development does not support varying soil properties for different sub-grid landunits. We also directly  
176 apply the snow accumulation physics in the CLM rather than customizing the snow density. By default,  
177 the current model does not form thermokarst lakes as the meltwater from excess ice melt becomes surface  
178 runoff and is removed from the grid cell. To apply the sub-grid representation, we initialize the case with  
179 three landunits (the triple-landunit case) that respectively represent the three terraces in the Lena river  
180 delta. We also initialize an “average ice single-landunit” case without the sub-grid representation of  
181 excess ice. The excess ice amount for each soil layer in the average ice single-landunit case is initially  
182 the same as that in the triple-landunit case. The volumetric content of excess ice is determined by spatial  
183 averaging those for three excess ice landunits in the triple-landunit case. Detailed information on the  
184 applied excess ice conditions for both cases is listed in Table 1.

185 We employed the single-point forcing data from in Westermann et al. (2016) for the Lena river delta  
186 from 1901 to 2100, which is based on the CRU-NCEP (<http://dods.extra.cea.fr/data/p529viov/cruncep/>)  
187 data set for the historical period (1901-2005) and the CCSM4 model output under the RCP4.5 scenario  
188 for the projected period (2006-2100), but downscaled with in-situ observations. We run 100-year spin-  
189 up simulations in order to stabilize the permafrost thermal regime after adding excess ice. Spin-up  
190 simulations are produced by running the model with cycled 1901-1920 climatological data. The purpose  
191 of spin-up simulations is to stabilize ground temperatures and volumes of excess ice bodies. The 100-  
192 year length for spin-up is sufficient, as the model is run in Satellite Phenology (SP) mode that does not  
193 involve slowly evolving biogeochemical processes such as soil carbon accumulation. Moreover, we  
194 address idealized single-point simulations for additional permafrost locations with both continental and  
195 maritime climate that showcase the difference to Lee et al. (2014), the results of which are included in  
196 the Supplementary material.

### 197 **2.3 Global simulations of excess ice melt**

198 The information available for the spatial distribution of excess ice and associated cryostratigraphies  
199 on the global scale is generally not as detailed as in the Lena river delta due to the lack of observations.  
200 For our global simulations we employ the widely used “Circum-Arctic Map of Permafrost and Ground-  
201 Ice Conditions” (hereafter the CAPS data; Brown et al., 2002) as data source, while we translate the  
202 ground ice condition in the CAPS data to different excess ice stratigraphies as model input data. The  
203 CAPS permafrost map categorizes the global permafrost area into classes coded by three factors (i)  
204 permafrost extent (c = continuous, d = discontinuous, s = sporadic, and i = isolated), (ii) visible ground  
205 ice content (h = high, m = medium, and l = low), and (iii) terrain and overburden (f = lowlands, highlands,  
206 and intra- and intermontane depressions characterized by thick overburden cover, and r = mountains,  
207 highlands ridges, and plateaus characterized by thin overburden cover and exposed bedrock), resulting  
208 in more than 20 different varieties in permafrost characteristics (Figure 2). For the simulations, we only  
209 use the CAPS distinction between the three classes: high, medium and low ice contents. We qualitatively  
210 categorize excess ice types with typical cryostratigraphies for which observations are available,  
211 recognizing that this is a crude first-guess of the global distribution of ground ice which needs to be  
212 improved in future studies.

213 The high ice CAPS classes (e.g. chf, chr, and dhf) in central and eastern Siberia, as well as in Alaska,  
214 partly coincide with Yedoma regions (Kanevskiy et al., 2011; Grosse et al., 2013). The cryostratigraphy  
215 of the high ice landunit is therefore broadly oriented at the excess ice contents and distribution in intact  
216 Yedoma, which is characterized by massive ice wedges leading to typical average volumetric content of  
217 total ground ice in the range from 60% to 90% (Schwamborn et al., 2002; Kanevskiy et al., 2011). We  
218 therefore set the volumetric content of excess ice in the high ice landunit to 70%, and we put excess ice  
219 in all the soil layers between 0.2 metres below the active layer and the bottom of hydrologically active  
220 soil layer (8.5 metres). The onset depth of the excess ice just below the active layer is based on the  
221 assumption of active ice aggradation which occurs at or below the permafrost table, e.g. the formation of  
222 wedge or segregation ice. Initializing high excess ice content throughout the whole soil layer imitates the

223 cryostratigraphy of Yedoma type ice, while roughly 65% of the high ice landunit is located out of the  
224 observed Yedoma regions (Schuur et al., 2015). The effects, limitations, and potential improvements of  
225 this initialization scenario will be mentioned in the discussion section. For the low ice landunit, we  
226 assume both a significantly lower volumetric excess ice content and a smaller vertical extent of the excess  
227 ice body. The volumetric excess ice content is set to 25%, and we add excess ice at soil layers within 0.2  
228 to 1.2 metres below the active layer, which in particular represents sediments with segregated ice (e.g.  
229 Cable et al., 2018), but also accounts for a wide range of different excess ice conditions found throughout  
230 the permafrost domain. For the mid ice landunit, we set the volumetric excess ice content to 45% and  
231 put excess ice within 0.2 to 2.2 metres below the active layer, making the volumetric excess ice content  
232 and vertical extent of which in between those for the low and high ice landunits. The cryostratigraphies  
233 determine that excess ice melt in the low ice landunit can result in a maximum of 0.36 metres of surface  
234 subsidence, while excess ice melt in the medium ice landunit can result in a maximum of 1.78 m of  
235 surface subsidence. For the high ice landunit, the surface subsidence can be more than 10 metres if all  
236 excess ice melts, which is expected to vary in space because of the different active layer thickness. For  
237 all three landunits, the active layer thickness is determined by the soil temperature profile by the end of  
238 the spinup in a no ice case, which is the simulation by the original CLM5 model without excess ice  
239 incorporated. Non-permafrost regions in the CAPS data are assigned the no ice landunit for 100% of  
240 their area. We emphasize that the prescribed cryostratigraphies are a first-order approximation that can  
241 by no means represent the wide variety of true ground ice conditions found in the permafrost domain.  
242 Nevertheless, this makes it possible to gauge the effect of excess ice melt on future projections of the  
243 permafrost thermal regime, when compared to “traditional” reference simulations without excess ice.

244 We design a tiling scheme prescribing the assignment of landunits for each CAPS class based on  
245 previous observations and empirical estimates (Table 2). All CAPS classes in this study are categorized  
246 into three levels of volumetric ice content (5%, 15%, and 25%) that are converted from the ranges (<10%,  
247 10-20%, and >20%) in the original CAPS data. The goal of our tiling scheme is to determine a  
248 combination of area weights of three excess ice landunits for each CAPS class, making the spatially  
249 averaged volumetric content of excess ice the same as that for the CAPS class. We assume that all CAPS  
250 classes have the same area fraction (20%) of the low ice landunit, and the CAPS classes with a higher  
251 ice content are due to the existence of the landunits with a higher content excess ice. We make this  
252 assumption based on previous studies that the segregated ice is widely distributed in permafrost.  
253 Observational studies have found segregated ice bodies in various continuous permafrost regions across  
254 the circum-arctic including West Central Alaska (Kanevskiy et al., 2014), Nunavik, Canada (Calmels  
255 and Allard, 2008), and Svalbard (Cable et al., 2018). In discontinuous permafrost regions, segregated ice  
256 bodies also commonly exist underneath Palsas and Lithasas, including Fennoscandia (Seppälä, 2011),  
257 Altai and Sayan, Russia (Iwanhama et al., 2012), Himalayas (Wünnemann et al., 2008), and Mongolia  
258 (Sharkhuu et al., 1999). The volumetric content of visible segregated ice bodies mentioned above ranges  
259 widely from 10-50% (Gilbert et al., 2016).

260 Given the tiling scheme prescribed above, all CAPS classes are assigned a 20% area of low ice  
261 landunit. Correspondingly, the CAPS classes with 15% volumetric ice content are assigned another 14%

262 area weight for mid ice landunit on top of the CAPS classes with 5% volumetric ice content, while the  
263 CAPS classes with 25% volumetric ice are assigned another 22% area for high ice landunit on top of the  
264 CAPS classes with 15% volumetric ice content. The classes of “chf” and “chr” are the exceptions as their  
265 corresponding regions are typically with the landscape of Yedoma or ice wedge polygonal tundra or both  
266 (Kanevskiy et al., 2011; Gross et al., 2013). We therefore assign only the low and high ice landunits for  
267 these two CAPS classes. Summing up the landunit fractions for all the CAPS grid cells within each CLM  
268 grid cell obtains the area weights on the grid level that are stored in the surface data file. Figure 3 shows  
269 a schematic plot for the initialization scenario and the area covered by different excess ice landunits as  
270 the result of sub-grid excess ice initialization in the global simulation case. Note that excess ice for some  
271 regions (e.g. Southern Norway and the Alps) can completely melt out during the spinup period since the  
272 CLM initial condition prescribes overly warm (non-permafrost) soil temperature for these regions.

273 In this study, we define the grid cells or landunits with permafrost as the ones having at least one  
274 hydrologically active soil layer that has been frozen in the last consecutive 24 months. In this case, we  
275 define fully degraded permafrost when all landunits in one grid cell have an active layer thickness of  
276 more than 6.5 metres, recognizing that in reality permafrost at many localities may continue to exist ~~at~~  
277 to greater depths. We also prepare a “grid-average ice case” by applying the same total amount of excess  
278 ice as in the sub-grid ice case in each soil layer, but using only one landunit instead of three that account  
279 for the sub-grid variability of excess ice. The volumetric content of excess ice in the single landunit is  
280 calculated as the spatial average of those in the three landunits in the triple-landunit case. This grid-  
281 average ice case provides a reference to evaluate the effects of the sub-grid excess ice representation on  
282 the global scale. Finally, we simulate a reference case without excess ice, denoted the “no ice case” in  
283 the following. Details on the three cases for the global simulations are listed in Table 3. All global cases  
284 are forced by the 3<sup>rd</sup> version of Global Soil Wetness Project forcing data (GSWP3; Kim et al., 2012),  
285 running in the Satellite Phenology (SP) mode. The International Land Atmosphere Model Benchmarking  
286 (ILAMB; Collier et al., 2018) project has indicated the superior performance of GSWP3 data forcing the  
287 CLM5 in the SP-only mode  
288 ([http://webext.cgd.ucar.edu/I20TR/\\_build\\_090817\\_CLM50SPONLY\\_CRUNCEP\\_GSWP3\\_WFDEI/in](http://webext.cgd.ucar.edu/I20TR/_build_090817_CLM50SPONLY_CRUNCEP_GSWP3_WFDEI/index.html)  
289 [dex.html](http://webext.cgd.ucar.edu/I20TR/_build_090817_CLM50SPONLY_CRUNCEP_GSWP3_WFDEI/index.html)). We conducted a 100-year spin-up using the 1901-1920 climatology before conducting  
290 historical period simulations covering 1901-2005. The anomaly forcing under the RCP8.5 scenario on  
291 top of the 1982-2005 climatology forces simulations in the projected period.

## 292 3. Results

### 293 3.1 Excess ice melt simulations for Lena River delta cryostratigraphies

294 By the end of the spinup in the triple-landunit case, the active layer thickness is 0.85 m, 0.55 m, and  
295 0.45 m for the ice-poor terrain, the Holocene ice wedge terrain, and the Yedoma ice complex, respectively.  
296 On the other hand, the active layer thickness for the average ice single-landunit case is 0.85 m, which is  
297 the same as in the no excess ice terrain in the triple-landunit case. For the average ice single-landunit  
298 case, a small amount of excess ice ( $24 \text{ kg m}^{-2}$ ) melts during the spinup period, resulting in 2.6 cm surface  
299 subsidence throughout the grid.



300 For the Yedoma ice complex, very little excess ice melt in the 1950s, and it stabilizes afterwards  
301 until the late 2000s when substantial ice melt and surface subsidence starts to occur. For the Holocene  
302 ground ice terrain, there is no excess ice melt before the late 2010s. By the year 2100, the Yedoma ice  
303 complex has exhibited nearly 4 metres of surface subsidence, while the Holocene ground ice terrain has  
304 about 0.6 metres of surface subsidence (Figure 4). For the average ice single-landunit case, the noticeable  
305 excess ice melt and surface subsidence starts in the late 2010s, which creates about 0.5 metres of surface  
306 subsidence by 2100. The magnitude of surface subsidence in the average ice single-landunit case is lower  
307 than both the Holocene ground ice terrain and the Yedoma ice complex in the triple-landunit case.

308 On the grid scale, the total excess ice melt is higher in the average ice single-landunit case than in  
309 the triple-landunit case (Figure 5). By the year 2100, the average ice single-landunit case has about 30  
310  $\text{kg m}^{-2}$  more excess ice melt than the triple-landunit case. The difference in excess ice on the grid level  
311 results from the different volumetric content of excess ice caused by the spatial averaging. In this way,  
312 the sub-grid representation of excess ice can potentially also provide more detailed and realistic  
313 representation of model variables on the grid level. This is particularly important for the CLM5, which  
314 serves as the land component in Earth System Models, which requires the coupling between interacting  
315 components on the grid level.

316 Compared to Westermann et al. (2016), the CLM5 with sub-grid excess ice simulates slightly less  
317 ( $\sim 20\%$  less) surface subsidence by 2100 for both the central delta and ice complex. We consider this a  
318 good agreement as we do not expect a closer fit of the model results due to substantial differences in the  
319 model physics (for example, the Cryogrid3 simulations in Westermann et al. (2016) lack a representation  
320 of the subsurface water cycle). What is in common between these two studies is the earlier start of excess  
321 ice melt and more surface subsidence in the ice complex than in the central delta. The CLM5 with sub-  
322 grid excess ice also exhibits the varying active layer thickness with different excess ice conditions as  
323 Cryogrid3 does. These results suggest that the new model development enables small-scale variability in  
324 excess ice melt and subsequent impacts in agreement with previously published modeling efforts.

### 325 **3.2 Global projection of permafrost thaw and excess ice melt**

326 Single-point simulations have shown that the varying excess ice cryostratigraphies for different  
327 landunits result in sub-grid variabilities of excess ice melt and surface subsidence under the warming  
328 climate. The same features remain in the sub-grid ice case within the global simulations that excess ice  
329 in the low ice landunit can completely melt out throughout the circum-Arctic permafrost region by the  
330 end of the 21<sup>st</sup> century (Figure 6). The modeled magnitude of surface subsidence is similar to the  $\sim 10$  cm  
331 surface subsidence observed in Barrow and West Dock in the early 21st century (Shiklomanov et al.,  
332 2013; Streleskiy et al., 2017). The magnitude of surface subsidence is also comparable to the 1-4 cm  
333  $\text{decade}^{-1}$  surface subsidence rate on average over the North Slope of Alaska observed by satellite  
334 measurements since the 1990s (Liu et al., 2010). In comparison, the absence of surface subsidence for  
335 Arctic Alaska modeled by Lee et al. (2014) is due to an overly deep (1 m deep) excess ice initialization  
336 depth. By the year 2100, most ice in the medium ice landunit melts away in the sub-arctic region, while  
337 there is less ice melt in the colder regions such as the North Slope of Alaska and the central Siberia. The

338 high ice landunit has the greatest surface subsidence among the three because of its high excess ice  
339 content, leading to 2-5 metres of surface subsidence by the year 2100.

340 The existence of excess ice modulates the thermal regime of permafrost soil and is a major control  
341 on permafrost degradation trajectories in a warming climate. Permafrost with excess ice consistently  
342 exhibits delayed permafrost degradation compared to the no ice case (Figure 7). For the no ice case  
343 modeled by the original CLM5, more than half of the permafrost area undergoes degradation by the end  
344 of the 21<sup>st</sup> century. By 2100, the only areas where permafrost remains are the North Slope of Alaska,  
345 Northern Canada, and the majority of the land area in Northern Siberia. The areas with remaining  
346 permafrost in the year 2100 under the RCP8.5 scenarios are substantially larger compared to the CLM4  
347 simulations, in which nearly all permafrost in Eurasia becomes degraded (Lawrence et al., 2012). For the  
348 grid-average ice case, the presence of excess ice stabilizes the permafrost thermal regime and thus  
349 sustains a larger permafrost area on a global scale in the simulation. For example, permafrost areas in  
350 some subarctic regions in the eastern and western Siberia, as well as part of the Arctic coastal regions in  
351 Yukon Territory, Canada, remain in the grid-average ice case by 2100. Compared to the grid-average ice  
352 case, even more permafrost areas are sustained in the sub-grid ice case, most of which are located in  
353 southern Siberia. In the subarctic regions in Alaska and Northwest Canada as well as part of the central  
354 Siberia, permafrost degradation is delayed from the 2040s in the grid ice case to the 2080s in the sub-  
355 grid ice case. We emphasize that permafrost is only sustained according to the accepted temperature-  
356 based definition (ground material at temperature below zero for two consecutive years), but excess ice  
357 continuously melts in this process, which energetically is a different mode of permafrost degradation,  
358 similar to a negative mass balance of glaciers and ice sheets.

359 In the sub-grid ice case, the landunits with high excess ice contents lead to more grid cells for which  
360 permafrost conditions remain in the year 2100 compared to the grid-average ice case. On the other hand,  
361 permafrost with excess ice only covers a fraction of a grid cell. Among the permafrost degradation  
362 trajectories in the three global simulation cases (Figure 8), the sub-grid ice case can provide a more  
363 detailed picture on the timing of permafrost degradation. Grid cells become ‘partially degraded  
364 permafrost’ if landunits with excess ice still contain permafrost, which phenomenologically is a more  
365 realistic representation that also makes it possible to represent the permafrost distribution in the  
366 discontinuous and sporadic permafrost zones. On the other hand, only “fully degraded permafrost” and  
367 “remaining permafrost” can be distinguished for the no ice and grid-average ice case. Under the warming  
368 climate in the 21<sup>st</sup> century, the existence of excess ice, especially the high content of excess ice, has a  
369 stabilizing effect on soil temperature that delay the disappearance of permafrost on the sub-grid level.  
370 Therefore, by the year 2100, there are regions with partially degraded permafrost in between intact and  
371 degraded permafrost (Figure 8). For example, in western Siberia, the Pacific coastal area of eastern  
372 Siberia, Northwestern Canada, and along the Brooks Range in Alaska, taliks form for landunits with low  
373 excess ice contents which leads to partially degraded permafrost regions. Therefore, permafrost  
374 degradation exhibits a gradual transition from continuous to discontinuous permafrost, and to non-  
375 permafrost regions. Some of these regions also encounter substantial surface subsidence in the high ice  
376 landunit (> 5 m) (Figure 6).

377 We further compare the total permafrost area (defined as landunits with active layer thickness < 6.5  
378 metres) in the three cases throughout time. The differences in permafrost area increase from the grid-  
379 average ice case and sub-grid ice case to the no ice case at a rate of 1000 km<sup>2</sup> per year until 2050 (Figure  
380 9). After 2050, the area difference of permafrost in the grid-average ice case and no ice cases rapidly  
381 increases, which reaches nearly one million km<sup>2</sup> by 2100. In the sub-grid ice case, the rate of increase  
382 remains relatively unchanged after 2050, resulting in an about 0.2 million km<sup>2</sup> larger permafrost area  
383 than that in the no ice case.

#### 384 4. Discussion

385 The aim of the sub-grid excess ice representation in the CLM5 is to facilitate long-term global  
386 projection of excess ice melt and surface subsidence in the permafrost regions. Results from our idealized  
387 sensitivity experiments (see supplemental material) implies that overly low volumetric content of excess  
388 ice, such as the grid-average ice case in this study and that in Lee et al. (2014), result in producing an  
389 overly early start of excess ice melt and an overly high melting rate. This is because the a higher content  
390 of excess ice covering a smaller area takes longer to absorb enough heat from the atmosphere to satisfy  
391 the latent heat of fusion requirements and absorb enough latent heat of fusion from the atmosphere before  
392 it can start melting. Consequently, a good model performance in this way relies not only on the updated  
393 sub-grid representation of excess ice in the global land model, but also on retrieving accurate initial  
394 conditions of excess ice. However, the corresponding observational data for both background excess ice  
395 conditions and model evaluation is sparse, considering especially that drastic excess ice melt as modeled  
396 until 2100 is only observed in few locations today (e.g. Günther et al., 2015). In the following, we discuss  
397 the challenges and limitations of the sub-grid excess ice framework, and how this sub-grid representation  
398 can potentially help the development of other CLM components. Both single-point and global test  
399 simulations in this study have shown that excess ice melts under a warming climate is sensitive to its  
400 initialization depth. The active-layer-dependent excess ice initialization in this study in the global  
401 simulation (sub-grid excess ice case) yields excess ice melt and surface subsidence rates in the early  
402 2000s that are comparable to observations. The lower depths of the assumed excess ice body control the  
403 termination of excess ice melt which at the same time determines the onset of talik formation in many  
404 permafrost areas. Due to the scarcity of observational data, it is unclear to what extent the  
405 cryostratigraphies assumed in our tiling scheme can reproduce the true vertical extent of excess ice bodies  
406 at least in a statistical sense. Even so, we manage to make the prescribed excess ice condition as close to  
407 the previous results as possible. Firstly, our tiling scheme on the large scale strictly follows the CAPS  
408 data (Brown et al., 2002) in terms of the volumetric excess ice content. Furthermore, statistics by Zhang  
409 et al. (2000) suggest the ranges of the vertical extent of ice-rich permafrost of 0-2 metres and 2-4 metres  
410 respectively for the CAPS classes with low (5%) and medium (15%) ice content. Comparatively, the  
411 vertical extents permafrost with excess ice prescribed by our tiling scheme are respectively 1.36 metres  
412 and 3.78 metres for the same CAPS classes, both of which lie within the ranges in Zhang et al. (2000).  
413 The vertical extent of ice-rich permafrost for the high ice landunit is much higher than that (4-6 metres)  
414 in Zhang et al. (2000), but the unmelted part of the ice bodies does not strongly affect the overall rate of  
415 excess ice melt, although the remaining ice can slightly change soil temperature and moisture of the

416 surrounding permafrost. We therefore imply that our high ice landunit initialization would not induce a  
417 strong bias in excess ice melt projection in the 21st century.

418 Due to the lack of excess ice datasets and observational evidence, our projections of excess ice melt  
419 and surface subsidence likely have biases that arise from the need to make empirical estimates and  
420 simplifications for the excess ice initialization scenarios in the global simulation cases. For example, as  
421 the CAPS data is mostly based on visible ice bodies (i.e., not pore ice) (Heginbottom et al., 1995), we  
422 used the reported volumetric ground ice content in the CAPS data to approximate the volumetric content  
423 of excess ice during model initialization. ~~F~~Further, the determination of volumetric contents of excess ice  
424 for three landunits also results from sparse observations and empirical estimates. The prescribed excess  
425 ice cryostratigraphies ignore ice morphology and the variation of volumetric content of excess ice with  
426 soil depth, regarding excess ice as homogeneous within each assigned sub-grid ice content type (low,  
427 mid, or high) (Figure 3, upper panel).. For the high ice landunit, we simplify the cryostratigraphy  
428 initialization to Yedoma type ice, which prescribes overly thick excess ice bodies out of the Yedoma  
429 regions (Schurr et al., 2015). A deficiency in the current version of source code prevents us from  
430 initializing non-Yedoma wedged ice for the high ice landunit where it occurs outside- of the Yedoma  
431 region. Future versions of our model development will have more freedom in the stratigraphic  
432 configuration of excess ice, which will make it possible to prescribe different cryostratigraphies of the  
433 same landunit (e.g. the high ice landunit) for different locations. Because of the above shortcomings in  
434 the excess ice initialization, we do not expect the modeled excess ice melt in this study to be an adequate  
435 representation of reality. ~~D~~However, direct ingestion of new or ~~improved—observational~~improved  
436 observational data sets of excess ice contents and cyostratigraphies would likely yield more accurate  
437 results. ~~however-However~~, a spatially distributed global dataset with quantitative information on excess  
438 ice stratigraphies does not exist at present. We emphasize that for a better projection of excess ice melt,  
439 more observational data of excess ice distribution and surface subsidence is required to further evaluate  
440 and validate the new model implementation of excess ice. On the regional scale, Jorgenson et al. (2008)  
441 presented a permafrost map of total ground ice volume for the uppermost 5 metres of permafrost based  
442 on both observations and estimates for Alaska. In addition, O’Neill et al. (2019) compiled permafrost  
443 maps for Northern Canada by paleographic modeling, mapping the abundances of three types of excess  
444 ice respectively. Further improvements of model results depend on additional observationally  
445 constrained datasets of excess ice conditions on the global scale.

446 The area weights of the excess ice landunits (Table 2) in the global simulation are obtained from the  
447 higher-resolution CAPS points located within a CLM grid cell. However, complex landscape  
448 development, such as thermokarst ponds, requires knowledge of the metre-scale distribution, for example  
449 the extent and geometry of individual ice wedges (Langer et al., 2016; Nitzbon et al., 2019), which cannot  
450 be represented with the still coarse-scale excess ice classes from the CAPS map. One possible solution  
451 to represent this could be to include another layer of sub-grid tiles below the CLM landunit level, where  
452 the individual tiles can interact laterally. This would allow for the representation of small-scale  
453 permafrost features within a large-scale landunit with a given excess ice content. An example of how this  
454 could work is given by Aas et al. (2019) who simulated both polygonal tundra and peat plateaus with a

455 two-tile interactive setup. This is also similar to the recent representation of hillslope hydrology by  
456 Swenson et al. (2019), where sub-grid tiles (on the column level in CLM) were used to represent different  
457 elements in a representative hillslope. In the future development of CLM, this could be part of a more  
458 generic tiling system where lateral heat and mass fluxes could be switched on and off to represent a wide  
459 range of land surface processes that are currently ignored or parameterized in LSMs. Fisher and Koven  
460 (2020) have discussed the challenges and opportunities in such an adaptive and generic tiling system.  
461 We would also advocate for enhancing current tiling schemes in such a direction, which could  
462 substantially improve the realism in the representation of permafrost landscapes in LSMs. However, the  
463 success of such a tiling approach will rely heavily on the availability of adequate observational data,  
464 further highlighting the need for observational efforts and close collaboration between field scientists  
465 and modelers.

466 The more detailed simulation of permafrost degradation trajectory with a sub-grid representation of  
467 excess ice also builds more potential on better modeling the permafrost-carbon feedback with  
468 biogeochemistry activated (CLM5BGC). Excess ice stabilizes the permafrost thermal regime, therefore  
469 alter the rate of carbon releasing from the permafrost (Shuur et al., 2008). Improved projections of  
470 permafrost warming could also enhance modeling of vegetation type changes (e.g. shrub expansion) that  
471 determines the nitrogen uptake to the atmosphere (Loranty and Goetz, 2012). On the other hand, the  
472 possibility to simulate surface subsidence and excess ice meltwater formation also opens the possibility  
473 of a more accurate representation of wetland formation. The increase in the area of wetland and soil  
474 moisture have an impact of the balance of CH<sub>4</sub> and CO<sub>2</sub> releasing from the permafrost as more organic  
475 matter could decompose in an anaerobic pathway (Lawrence et al., 2015; Treat et al., 2015). Compared  
476 to the parameterized inundated area simulation in the CLM5 (Ekici et al., 2019), a process-based wetland  
477 physics scheme together with the sub-grid representation of excess ice in this study would substantially  
478 contribute to the biogeochemical modeling over the circum-arctic area.

## 479 **5. Conclusion**

480 This study develops a sub-grid representation of excess ice in the CLM5 and examines the impacts  
481 of the existence and melting of excess ice in the sub-grid scale in a warming climate. Extra landunits  
482 duplicated from the natural vegetated landunit in the CLM sub-grid hierarchy make it possible to  
483 prescribe up to three different excess ice conditions in each grid cell with permafrost.

484 A test over the Lena river delta showcases that the sub-grid representation of excess ice can retrieve  
485 the sub-grid variability of annual thaw-freeze state and the excess ice melt and surface subsidence  
486 through time. On the other hand, initializing excess ice homogeneously throughout the grid cell produces  
487 a smaller stabilization effect of excess ice to the permafrost thermal regime and the local surface  
488 subsidence under a warming climate. With a tiling scheme ingesting a global data set of excess ice  
489 condition into the CLM surface data, our model development shows the capability of portraying more  
490 details on simulating permafrost degradation trajectories. As excess ice thermally stabilizes the  
491 permafrost on the sub-grid scale, permafrost degrades with a trajectory from continuous permafrost to  
492 discontinuous permafrost, and finally to a permafrost-free area. The modeled global pattern of permafrost

493 therefore exhibits regions of discontinuous permafrost as the transition zone between the continuous  
494 permafrost and degraded permafrost.

495 This study, for the first time, used an ESM to project excess ice melt and surface subsidence and  
496 permafrost degradation with sub-grid variability. The approach of duplicating tiles at the landunit level  
497 instead of the column level allows more freedom for further developments in this direction. Furthermore,  
498 the new CLM tiling hierarchy has much more potential than representing more accurate excess ice  
499 physics as examined in this study. The accuracies of predicted excess ice melt and surface subsidence  
500 trends are limited at present by the available global-scale dataset and studies on excess ground ice  
501 conditions, thus further advancement of the excess ice modeling will rely on new or improved  
502 observational studies or datasets of the excess ground ice conditions at the global scale. The model  
503 development in our study, therefore, lays the foundation for further advances focusing on excess ice  
504 modeling and other processes in the CLM framework that could benefit from an improved sub-grid  
505 representation.

506

#### 507 **Source code and data availability**

508 The original Community Land Model is available at <https://github.com/ESCOMP/ctsm>. The source code  
509 of model development in this study is available from the corresponding author upon request.

#### 510 **Author contributions**

511 L.C conducted model development work and wrote the initial draft with additional contributions from  
512 all authors. H.L, S.W, and K.S.A provided ideas and help during the process of model development. H.L  
513 provided the code of excess ice physics in the earlier version of CLM. L.C prepared all figures.

#### 514 **Acknowledgments**

515 This study is funded by the Research Council of Norway KLIMAFORSK program (PERMANOR;  
516 RCN#255331) and Research Council of Norway INFRASTRUKTUR program (INES; RCN#270061).  
517 ~~This study is funded by the Research Council of Norway KLIMAFORSK program (PERMANOR;~~  
518 ~~RCN#255331).~~—K.S.A is supported by the Research Council of Norway EMERALD project  
519 (RCN#294948). We thank Sarah Chadburn for helpful comments and suggestions in preparing this  
520 manuscript. We thank the editor and two anonymous reviewers for their great comments and helps that  
521 have improved this paper substantially.

522

#### 523 **Reference**

524 Aas, K. S., Martin, L., Nitzbon, J., Langer, M., Boike, J., Lee, H., Berntsen, T. K., and Westermann, S.:  
525 Thaw processes in ice-rich permafrost landscapes represented with laterally coupled tiles in a  
526 land surface model, *The Cryosphere*, 13, 591-609, 10.5194/tc-13-591-2019, 2019.

- 527 Brown, J., Ferrians Jr, O., Heginbottom, J., and Melnikov, E.: Circum-Arctic map of permafrost and  
528 ground-ice conditions, US Geological Survey Reston, VA, 1997.
- 529 Burke, E. J., Dankers, R., Jones, C. D., and Wiltshire, A. J.: A retrospective analysis of pan Arctic  
530 permafrost using the JULES land surface model, *Climate Dynamics*, 41, 1025-1038,  
531 10.1007/s00382-012-1648-x, 2013.
- 532 Cable, S., Elberling, B., and Kroon, A.: Holocene permafrost history and cryostratigraphy in the High-  
533 Arctic Adventdalen Valley, central Svalbard, *Boreas*, 47, 423-442, 10.1111/bor.12286, 2018.
- 534 Calmels, F., and Allard, M.: Segregated ice structures in various heaved permafrost landforms through  
535 CT Scan, *Earth Surface Processes and Landforms*, 33, 209-225, 10.1002/esp.1538, 2008.
- 536 Collier, N., Hoffman, F. M., Lawrence, D. M., Keppel-Aleks, G., Koven, C. D., Riley, W. J., Mu, M.,  
537 and Randerson, J. T.: The International Land Model Benchmarking (ILAMB) system: design,  
538 theory, and implementation, *Journal of Advances in Modeling Earth Systems*, 10, 2731-2754,  
539 2018.
- 540 Ekici, A., Lee, H., Lawrence, D. M., Swenson, S. C., and Prigent, C.: Ground subsidence effects on  
541 simulating dynamic high-latitude surface inundation under permafrost thaw using CLM5,  
542 *Geosci. Model Dev.*, 12, 5291-5300, 10.5194/gmd-12-5291-2019, 2019.
- 543 Fedorova, I., Chetverova, A., Bolshiyarov, D., Makarov, A., Boike, J., Heim, B., Morgenstern, A.,  
544 Overduin, P. P., Wegner, C., Kashina, V., Eulenburg, A., Dobrotina, E., and Sidorina, I.: Lena  
545 Delta hydrology and geochemistry: long-term hydrological data and recent field observations,  
546 *Biogeosciences*, 12, 345-363, 10.5194/bg-12-345-2015, 2015.
- 547 Fisher, R. A., and Koven, C. D.: Perspectives on the future of Land Surface Models and the challenges  
548 of representing complex terrestrial systems, *Journal of Advances in Modeling Earth Systems*,  
549 n/a, 10.1029/2018MS001453, 2020.
- 550 Fritz, M., Wetterich, S., Meyer, H., Schirrmeyer, L., Lantuit, H., and Pollard, W. H.: Origin and  
551 characteristics of massive ground ice on Herschel Island (western Canadian Arctic) as revealed  
552 by stable water isotope and Hydrochemical signatures, *Permafrost and Periglacial Processes*, 22,  
553 26-38, 10.1002/ppp.714, 2011.
- 554 Gilbert, G. L., Kanevskiy, M., and Murton, J. B.: Recent Advances (2008–2015) in the Study of Ground  
555 Ice and Cryostratigraphy, *Permafrost and Periglacial Processes*, 27, 377-389, 10.1002/ppp.1912,  
556 2016.
- 557 Grosse, G., Romanovsky, V., Jorgenson, T., Anthony, K. W., Brown, J., and Overduin, P. P.:  
558 Vulnerability and feedbacks of permafrost to climate change, *Eos, Transactions American*  
559 *Geophysical Union*, 92, 73-74, 2011.
- 560 Grosse, G., Robinson, J. E., Bryant, R., Taylor, M. D., Harper, W., DeMasi, A., Kyker-Snowman, E.,  
561 Veremeeva, A., Schirrmeyer, L., and Harden, J.: Distribution of late Pleistocene ice-rich

562 syngenetic permafrost of the Yedoma Suite in east and central Siberia, Russia, US Geological  
563 Survey Open File Report, 2013, 1-37, 2013.

564 Günther, F., Overduin, P. P., Yakshina, I. A., Opel, T., Baranskaya, A. V., and Grigoriev, M. N.:  
565 Observing Muostakh disappear: permafrost thaw subsidence and erosion of a ground-ice-rich  
566 island in response to arctic summer warming and sea ice reduction, *The Cryosphere*, 9, 151-178,  
567 10.5194/tc-9-151-2015, 2015.

568 Heginbottom, J.A., Dubreuil, M.A. and Harker, P.A.: Canada, Permafrost. National Atlas of Canada.  
569 Natural Resources Canada, 5th Edition, MCR, 4177, 1995.

570 Hugelius, G., Strauss, J., Zubrzycki, S., Harden, J. W., Schuur, E. A. G., Ping, C. L., Schirmer, L.,  
571 Grosse, G., Michaelson, G. J., Koven, C. D., O'Donnell, J. A., Elberling, B., Mishra, U., Camill,  
572 P., Yu, Z., Palmtag, J., and Kuhry, P.: Estimated stocks of circumpolar permafrost carbon with  
573 quantified uncertainty ranges and identified data gaps, *Biogeosciences*, 11, 6573-6593,  
574 10.5194/bg-11-6573-2014, 2014.

575 Kanevskiy, M., Shur, Y., Fortier, D., Jorgenson, M. T., and Stephani, E.: Cryostratigraphy of late  
576 Pleistocene syngenetic permafrost (yedoma) in northern Alaska, Itkillik River exposure,  
577 *Quaternary Research*, 75, 584-596, 10.1016/j.yqres.2010.12.003, 2011.

578 Iwahana, G., Fukui, K., Mikhailov, N., Ostanin, O., and Fujii, Y.: Internal Structure of a Lithalsa in the  
579 Akkol Valley, Russian Altai Mountains, 23, 107-118, 10.1002/pp

580 Jorgenson, M., Yoshikawa, K., Kanevskiy, M., Shur, Y., Romanovsky, V., Marchenko, S., Grosse, G.,  
581 Brown, J., and Jones, B.: Permafrost characteristics of Alaska, *Proceedings of the Ninth*  
582 *International Conference on Permafrost*, 2008, 121-122.p.1734, 2012.

583 Kanevskiy, M., Jorgenson, T., Shur, Y., O'Donnell, J. A., Harden, J. W., Zhuang, Q., and Fortier, D.:  
584 Cryostratigraphy and Permafrost Evolution in the Lacustrine Lowlands of West-Central Alaska,  
585 *Permafrost and Periglacial Processes*, 25, 14-34, 10.1002/ppp.1800, 2014.

586 Kim, H., Yoshimura, K., Chang, E., Famiglietti, J., and Oki, T.: Century long observation constrained  
587 global dynamic downscaling and hydrologic implication, *AGU Fall Meeting Abstracts*, 2012.

588 Kokelj, S. V., Lacelle, D., Lantz, T. C., Tunnicliffe, J., Malone, L., Clark, I. D., and Chin, K. S.: Thawing  
589 of massive ground ice in mega slumps drives increases in stream sediment and solute flux across  
590 a range of watershed scales, *Journal of Geophysical Research: Earth Surface*, 118, 681-692,  
591 10.1002/jgrf.20063, 2013.

592 Koven, C. D., Ringeval, B., Friedlingstein, P., Ciais, P., Cadule, P., Khvorostyanov, D., Krinner, G., and  
593 Tarnocai, C.: Permafrost carbon-climate feedbacks accelerate global warming, *Proceedings of*  
594 *the National Academy of Sciences*, 108, 14769-14774, 2011.

595 Langer, M., Westermann, S., Boike, J., Kirillin, G., Grosse, G., Peng, S., and Krinner, G.: Rapid  
596 degradation of permafrost underneath waterbodies in tundra landscapes—toward a



597 representation of thermokarst in land surface models, *Journal of Geophysical Research: Earth*  
598 *Surface*, 121, 2446-2470, 2016.

599 Langer, M., Westermann, S., Heikenfeld, M., Dorn, W., and Boike, J.: Satellite-based modeling of  
600 permafrost temperatures in a tundra lowland landscape, *Remote Sensing of Environment*, 135,  
601 12-24, <https://doi.org/10.1016/j.rse.2013.03.011>, 2013.

602 Lawrence, D. M., Slater, A. G., Romanovsky, V. E., and Nicolsky, D. J.: Sensitivity of a model projection  
603 of near-surface permafrost degradation to soil column depth and representation of soil organic  
604 matter, *Journal of Geophysical Research: Earth Surface*, 113, 10.1029/2007JF000883, 2008.

605 Lawrence, D. M., Oleson, K. W., Flanner, M. G., Thornton, P. E., Swenson, S. C., Lawrence, P. J., Zeng,  
606 X., Yang, Z. L., Levis, S., and Sakaguchi, K.: Parameterization improvements and functional  
607 and structural advances in version 4 of the Community Land Model, *Journal of Advances in*  
608 *Modeling Earth Systems*, 3, 2011.

609 Lawrence, D. M., Slater, A. G., and Swenson, S. C.: Simulation of present-day and future permafrost and  
610 seasonally frozen ground conditions in CCSM4, *Journal of Climate*, 25, 2207-2225, 2012.

611 Lawrence, D. M., Koven, C. D., Swenson, S. C., Riley, W. J., and Slater, A. G.: Permafrost thaw and  
612 resulting soil moisture changes regulate projected high-latitude CO<sub>2</sub> and CH<sub>4</sub> emissions,  
613 *Environmental Research Letters*, 10, 094011, 10.1088/1748-9326/10/9/094011, 2015.

614 Lawrence, D. M., Fisher, R. A., Koven, C. D., Oleson, K. W., Swenson, S. C., Bonan, G., Collier, N.,  
615 Ghimire, B., van Kampenhou, L., Kennedy, D., Kluzek, E., Lawrence, P. J., Li, F., Li, H.,  
616 Lombardozi, D., Riley, W. J., Sacks, W. J., Shi, M., Vertenstein, M., Wieder, W. R., Xu, C.,  
617 Ali, A. A., Badger, A. M., Bisht, G., van den Broeke, M., Brunke, M. A., Burns, S. P., Buzan,  
618 J., Clark, M., Craig, A., Dahlin, K., Drewniak, B., Fisher, J. B., Flanner, M., Fox, A. M., Gentine,  
619 P., Hoffman, F., Keppel-Aleks, G., Knox, R., Kumar, S., Lenaerts, J., Leung, L. R., Lipscomb,  
620 W. H., Lu, Y., Pandey, A., Pelletier, J. D., Perket, J., Randerson, J. T., Ricciuto, D. M.,  
621 Sanderson, B. M., Slater, A., Subin, Z. M., Tang, J., Thomas, R. Q., Val Martin, M., and Zeng,  
622 X.: The Community Land Model Version 5: Description of New Features, Benchmarking, and  
623 Impact of Forcing Uncertainty, 11, 4245-4287, 10.1029/2018ms001583, 2019.

624 Lee, H., Swenson, S. C., Slater, A. G., and Lawrence, D. M.: Effects of excess ground ice on projections  
625 of permafrost in a warming climate, *Environmental Research Letters*, 9, 124006, 2014.

626 Liu, L., Zhang, T., and Wahr, J.: InSAR measurements of surface deformation over permafrost on the  
627 North Slope of Alaska, *Journal of Geophysical Research: Earth Surface*, 115,  
628 10.1029/2009jf001547, 2010.

629 Loranty, M. M., and Goetz, S. J.: Shrub expansion and climate feedbacks in Arctic tundra, *Environmental*  
630 *Research Letters*, 7, 011005, 10.1088/1748-9326/7/1/011005, 2012.

631 Nitzbon, J., Langer, M., Westermann, S., Martin, L., Aas, K. S., and Boike, J.: Pathways of ice-wedge  
632 degradation in polygonal tundra under different hydrological conditions, *The Cryosphere*, 13,  
633 1089-1123, 10.5194/tc-13-1089-2019, 2019.

- 634 Nitzbon, J., Westermann, S., Langer, M., Martin, L. C. P., Strauss, J., Laboor, S., and Boike, J.: Fast  
635 response of cold ice-rich permafrost in northeast Siberia to a warming climate, *Nature*  
636 *Communications*, 11, 2201, 10.1038/s41467-020-15725-8, 2020.
- 637 O'Neill, H. B., Wolfe, S. A., and Duchesne, C.: New ground ice maps for Canada using a paleogeographic  
638 modelling approach, *The Cryosphere*, 13, 753-773, 10.5194/tc-13-753-2019, 2019.
- 639 Pascale, G. P. D., Pollard, W. H., and Williams, K. K. J. o. G. R. A.: Geophysical mapping of ground  
640 ice using a combination of capacitive coupled resistivity and ground-penetrating radar,  
641 *Northwest Territories, Canada*, 113, 2008.
- 642 Rachold, V., and Grigoriev, M.: Russian-German Cooperation SYSTEM LAPTEV SEA 2000: The Lena  
643 Delta 1998 Expedition, *Berichte zur Polarforschung (Reports on Polar Research)*, 315, 1999.
- 644 Schaefer, K., Lantuit, H., Romanovsky, V. E., Schuur, E. A. G., and Witt, R.: The impact of the  
645 permafrost carbon feedback on global climate, *Environmental Research Letters*, 9, 085003,  
646 10.1088/1748-9326/9/8/085003, 2014.
- 647 Schirrmeyer, L., Grosse, G., Schwamborn, G., Andreev, A. A., Meyer, H., Kunitsky, V. V., Kuznetsova,  
648 T. V., Dorozhkina, M. V., Pavlova, E. Y., Bobrov, A. A., and Oezen, D.: Late Quaternary  
649 History of the Accumulation Plain North of the Chekanovsky Ridge (Lena Delta, Russia): A  
650 Multidisciplinary Approach, *Polar Geography*, 27, 277-319, 10.1080/789610225, 2003.
- 651 Schirrmeyer, L., Grosse, G., Schnelle, M., Fuchs, M., Krbetschek, M., Ulrich, M., Kunitsky, V.,  
652 Grigoriev, M., Andreev, A., Kienast, F., Meyer, H., Babiy, O., Klimova, I., Bobrov, A.,  
653 Wetterich, S., and Schwamborn, G.: Late Quaternary paleoenvironmental records from the  
654 western Lena Delta, Arctic Siberia, *Palaeogeography, Palaeoclimatology, Palaeoecology*, 299,  
655 175-196, <https://doi.org/10.1016/j.palaeo.2010.10.045>, 2011.
- 656 Schirrmeyer, L., Froese, D., Tumskey, V., Grosse, G., and Wetterich, S.: Yedoma: Late Pleistocene ice-  
657 rich syngenetic permafrost of Beringia, in: *Encyclopedia of Quaternary Science*. 2nd edition,  
658 Elsevier, 542-552, 2013.
- 659 Schneider, J., Grosse, G., and Wagner, D.: Land cover classification of tundra environments in the Arctic  
660 Lena Delta based on Landsat 7 ETM+ data and its application for upscaling of methane  
661 emissions, *Remote Sensing of Environment*, 113, 380-391,  
662 <https://doi.org/10.1016/j.rse.2008.10.013>, 2009.
- 663 Schuur, E. A., Bockheim, J., Canadell, J. G., Euskirchen, E., Field, C. B., Goryachkin, S. V., Hagemann,  
664 S., Kuhry, P., Lafleur, P. M., and Lee, H.: Vulnerability of permafrost carbon to climate change:  
665 Implications for the global carbon cycle, *BioScience*, 58, 701-714, 2008.
- 666 Schuur, E. A. G., McGuire, A. D., Schädel, C., Grosse, G., Harden, J. W., Hayes, D. J., Hugelius, G.,  
667 Koven, C. D., Kuhry, P., Lawrence, D. M., Natali, S. M., Olefeldt, D., Romanovsky, V. E.,  
668 Schaefer, K., Turetsky, M. R., Treat, C. C., and Vonk, J. E.: Climate change and the permafrost  
669 carbon feedback, *Nature*, 520, 171, 10.1038/nature14338, 2015.

670 Schwamborn, G., Rachold, V., and Grigoriev, M. N.: Late Quaternary sedimentation history of the Lena  
671 Delta, *Quaternary International*, 89, 119-134, [https://doi.org/10.1016/S1040-6182\(01\)00084-2](https://doi.org/10.1016/S1040-6182(01)00084-2),  
672 2002.

673 Seppälä, M.: Synthesis of studies of palsa formation underlining the importance of local environmental  
674 and physical characteristics, *Quaternary Research*, 75, 366-370,  
675 <https://doi.org/10.1016/j.yqres.2010.09.007>, 2011.

676 Sharkhuu, N.: Occurrence of frost heaving in the Selenge River Basin, Mongolia, 10, 187-192,  
677 [10.1002/\(sici\)1099-1530\(199904/06\)10:2<187::Aid-ppp294>3.0.Co;2-w](https://doi.org/10.1002/(sici)1099-1530(199904/06)10:2<187::Aid-ppp294>3.0.Co;2-w), 1999.

678 Shiklomanov, N. I., Streletskiy, D. A., Little, J. D., and Nelson, F. E.: Isotropic thaw subsidence in  
679 undisturbed permafrost landscapes, *Geophysical Research Letters*, 40, 6356-6361,  
680 [10.1002/2013gl058295](https://doi.org/10.1002/2013gl058295), 2013.

681 Slater, A. G., and Lawrence, D. M.: Diagnosing present and future permafrost from climate models,  
682 *Journal of Climate*, 26, 5608-5623, 2013.

683 Streletskiy, D. A., Shiklomanov, N. I., Little, J. D., Nelson, F. E., Brown, J., Nyland, K. E., and Klene,  
684 A. E.: Thaw Subsidence in Undisturbed Tundra Landscapes, Barrow, Alaska, 1962–2015,  
685 *Permafrost and Periglacial Processes*, 28, 566-572, [10.1002/ppp.1918](https://doi.org/10.1002/ppp.1918), 2017.

686 Swenson, S. C., Clark, M., Fan, Y., Lawrence, D. M., and Perket, J.: Representing Intrahillslope Lateral  
687 Subsurface Flow in the Community Land Model, *Journal of Advances in Modeling Earth  
688 Systems*, 11, 4044-4065, [10.1029/2019MS001833](https://doi.org/10.1029/2019MS001833), 2019.

689 Treat, C. C., Natali, S. M., Ernakovich, J., Iversen, C. M., Lupascu, M., McGuire, A. D., Norby, R. J.,  
690 Roy Chowdhury, T., Richter, A., Šantrůčková, H., Schädel, C., Schuur, E. A. G., Sloan, V. L.,  
691 Turetsky, M. R., and Waldrop, M. P.: A pan-Arctic synthesis of CH<sub>4</sub> and CO<sub>2</sub> production from  
692 anoxic soil incubations, 21, 2787-2803, [10.1111/gcb.12875](https://doi.org/10.1111/gcb.12875), 2015.

693 Turetsky, M. R., Abbott, B. W., Jones, M. C., Anthony, K. W., Olefeldt, D., Schuur, E. A., Koven, C.,  
694 McGuire, A. D., Grosse, G., and Kuhry, P.: Permafrost collapse is accelerating carbon release,  
695 *Nature*, 569, 32-34, 2019.

696 Ulrich, M., Grosse, G., Chabrilat, S., and Schirrmeister, L.: Spectral characterization of periglacial  
697 surfaces and geomorphological units in the Arctic Lena Delta using field spectrometry and  
698 remote sensing, *Remote Sensing of Environment*, 113, 1220-1235,  
699 <https://doi.org/10.1016/j.rse.2009.02.009>, 2009.

700 Walter, K. M., Zimov, S. A., Chanton, J. P., Verbyla, D., and Chapin, F. S.: Methane bubbling from  
701 Siberian thaw lakes as a positive feedback to climate warming, *Nature*, 443, 71-75,  
702 [10.1038/nature05040](https://doi.org/10.1038/nature05040), 2006.

703 West, J. J., and Plug, L. J.: Time-dependent morphology of thaw lakes and taliks in deep and shallow  
704 ground ice, *Journal of Geophysical Research: Earth Surface*, 113, [10.1029/2006jf000696](https://doi.org/10.1029/2006jf000696), 2008.

705 Westermann, S., Langer, M., Boike, J., Heikenfeld, M., Peter, M., Eitzelmüller, B., and Krinner, G.:  
706 Simulating the thermal regime and thaw processes of ice-rich permafrost ground with the land-  
707 surface model CryoGrid 3, *Geosci. Model Dev.*, 9, 523-546, 10.5194/gmd-9-523-2016, 2016.

708 Wünnemann, B., Reinhardt, C., Kotlia, B. S., and Riedel, F.: Observations on the relationship between  
709 lake formation, permafrost activity and lithalsa development during the last 20 000 years in the  
710 Tso Kar basin, Ladakh, India, 19, 341-358, 10.1002/ppp.631, 2008.

711 Zhang, T., Barry, R. G., Knowles, K., Heginbottom, J. A., and Brown, J.: Statistics and characteristics  
712 of permafrost and ground-ice distribution in the Northern Hemisphere, *Polar Geography*, 23,  
713 132-154, 10.1080/10889379909377670, 1999.

714 Zhang, T., Heginbottom, J. A., Barry, R. G., and Brown, J.: Further statistics on the distribution of  
715 permafrost and ground ice in the Northern Hemisphere, *Polar Geography*, 24, 126-131,  
716 10.1080/10889370009377692, 2000.

717 Zimov, S. A., Schuur, E. A., and Chapin, F. S.: Permafrost and the global carbon budget, *Science*, 312,  
718 1612-1613, 2006.

719

720 **Table 1: The excess ice initialization scenario in each of the three terraces (landunits) for the Lena**  
 721 **River delta, as well as that for the single-landunit excess ice initialization case.**  
 722

Depth (after adding ice)	Volumetric Ice content	Area weight
No excess ice terrain		
N/A	0%	24.6%
Holocene ground ice terrain		
0.9-9 m	65%	66.6%
Yedoma ice complex		
0.6-20 m	90%	8.8%
Average ice single-landunit case		
0.6-0.9 m	7.92%	100%
0.9-9 m	51.21%	100%
9-20 m	7.92%	100%

723

724

725 **Table 2: The tiling scheme prescribing area weights of landunits for each CAPS class. The detailed**  
 726 **CAPS classes are shown in Figure 2.**

Overall visible ground ice content for each CAPS point	Tiling scheme (area weights for each excess ice category)	Eligible CAPS types
5%	80% no excess ice; 20% Low	clf; clf; slf; ilf; clr; dlr; slr; ilr
15%	58% no excess ice; 20% Low; 22% Medium	cmf; dmf; smf; imf; dhr; shr; ihr
15%	66% no excess ice; 20% Low; 14% High	chr
25%	44% no excess ice; 20% Low; 22% Medium; 14% High	dhf; shf; ihf
25%	52% no excess ice; 20% Low; 28% High	chf

727 Note: For each class, the first letter is for the permafrost extent, the second for the excess ice content, and the third  
 728 for the terrain and overburden, following Brown et al. (2002).

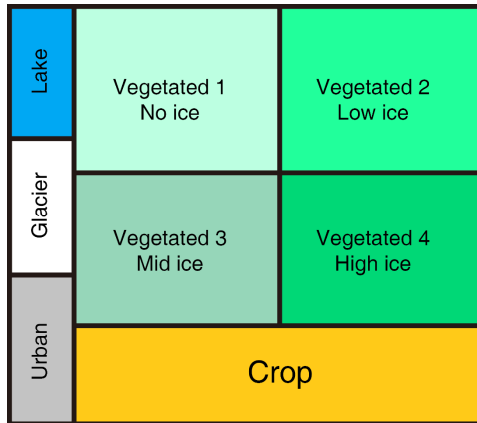
729

730 **Table 3: List of simulations conducted for this study.**

Cases	Description
Single point cases for the Lena river delta	
Triple-landunit case	Applying the sub-grid representation of excess ice. Three natural vegetated landunit initialized.
Average ice single-landunit case	Not applying the sub-grid representation of excess ice. Only one natural vegetated landunit initialized. The grid-mean excess ice content for each soil layer in the only landunit is calculated by spatially averaging those in different landunits in the triple-landunit case.
Global simulation cases	
No ice case	Not adding any excess ground ice (the original CLM5 simulation).
Sub-grid ice case	Applying the sub-grid representation of excess ice. A tiling scheme helps to “translate” excess ice conditions in the CAPS data to fit what the CLM5 requires.
Grid-average ice case	Not applying the sub-grid representation of excess ice. The grid-mean excess ice content for each soil layer is calculated by spatially averaging those in different landunits in the sub-grid ice case.

731

732

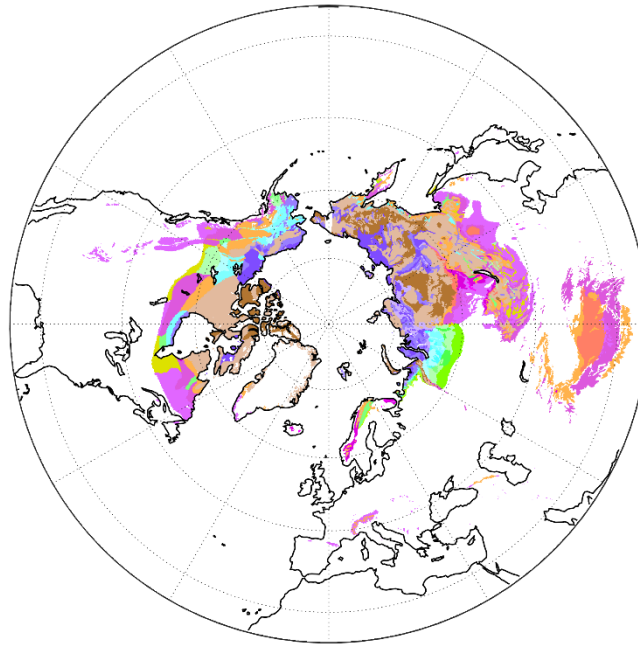


733

734 **Figure 1: Modification of the CLM5 tiling hierarchy on the landunit level containing four natural**  
 735 **vegetated landunits for different excess ice conditions.**

736





**Permafrost area classification**

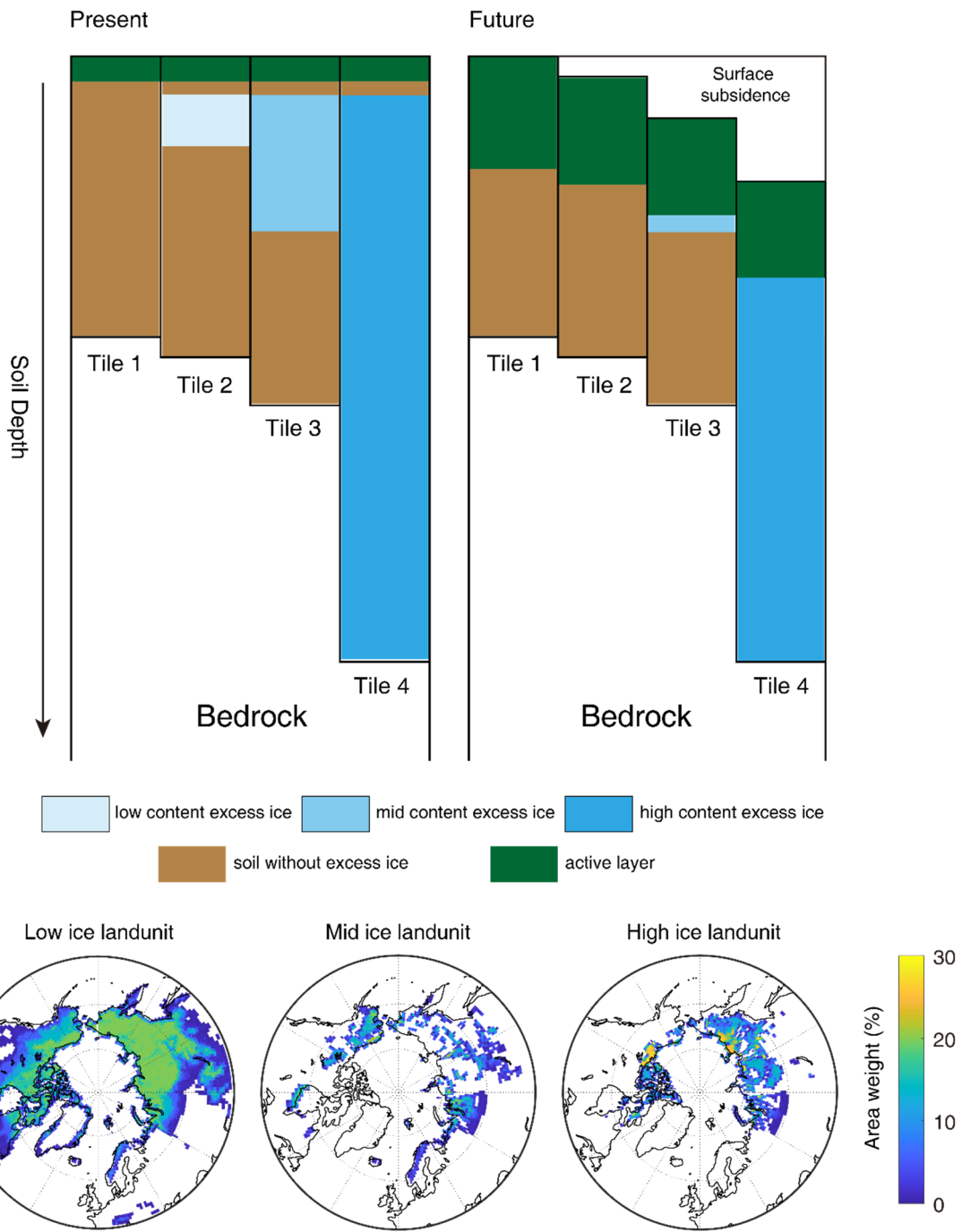
Permafrost Extent	Ground Ice Content (percent by volume)				
	Lowlands, highlands, and intra-and intermontane depressions			Mountains, highlands, ridges, and plateaus	
	25%	15%	5%	15%	5%
Continuous (100%)	chf	cmf	clf	chr	clr
Discontinuous (70%)	dhf	dmf	dlf	dhr	dhr
Sporadic (30%)	shf	smf	slf	shr	slr
Isolated (5%)	ihf	imf	ilf	ihr	ilr

\* Letter code naming: The first letter is for the permafrost extent, second for the ground excess ice concent, and the thrid for the terrain and overburden.

737

738 **Figure 2: Spatial distribution of excess ground ice in the Northern Hemisphere modified from**  
 739 **Brown et al. (2002). Compared to the original data, permafrost extents and ground ice contents**  
 740 **are converted to definite numbers (percentages) for model computation.**

741



743

744 **Figure 3. Schematic representation of the sub-grid excess ice initialization scenario, and maps**  
 745 **showing the area weight (%) occupied by different excess ice landunits, i.e. the initial condition of**  
 746 **excess ice in the global simulation.**

747

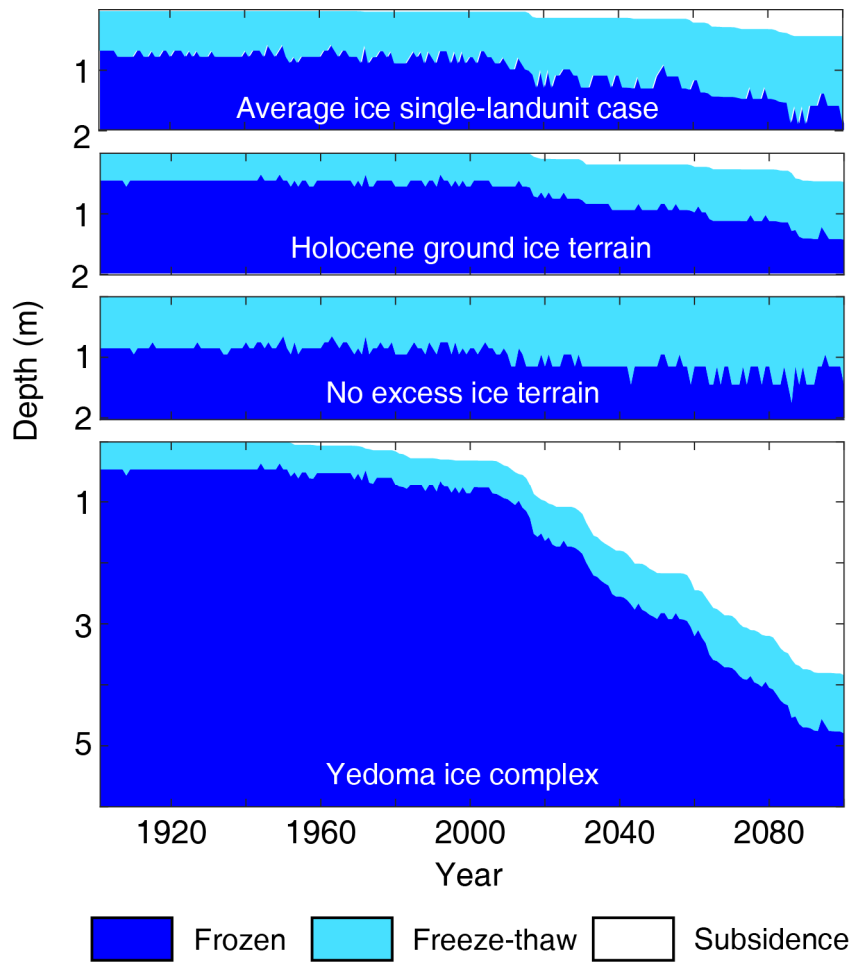
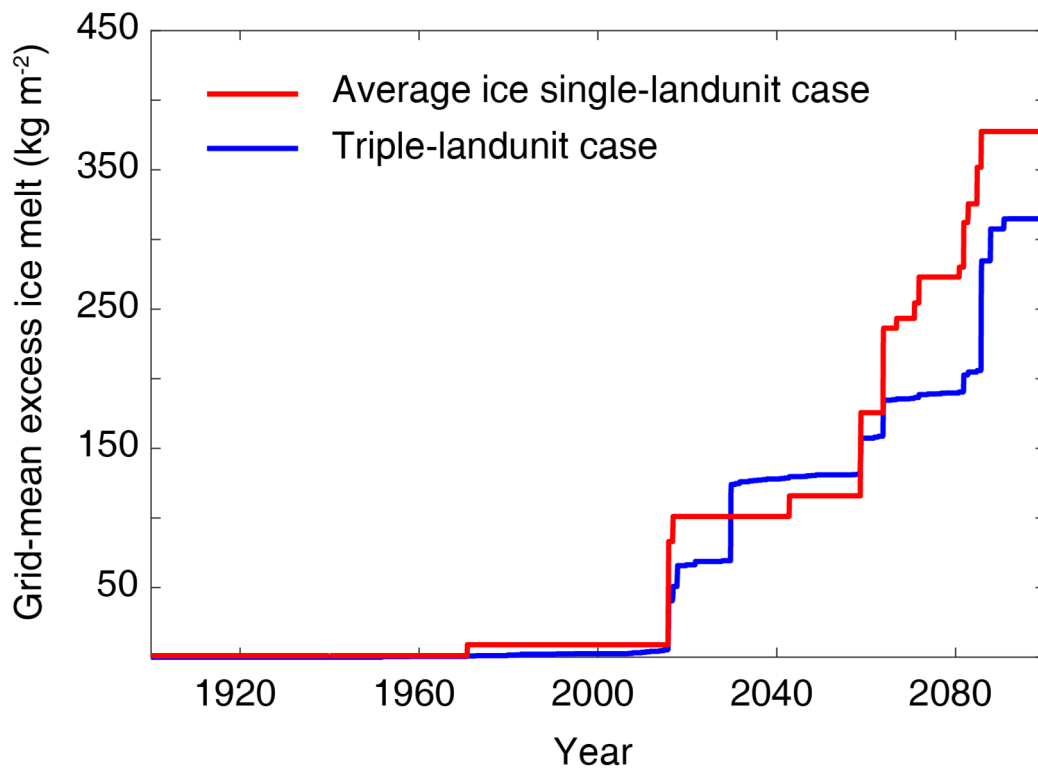


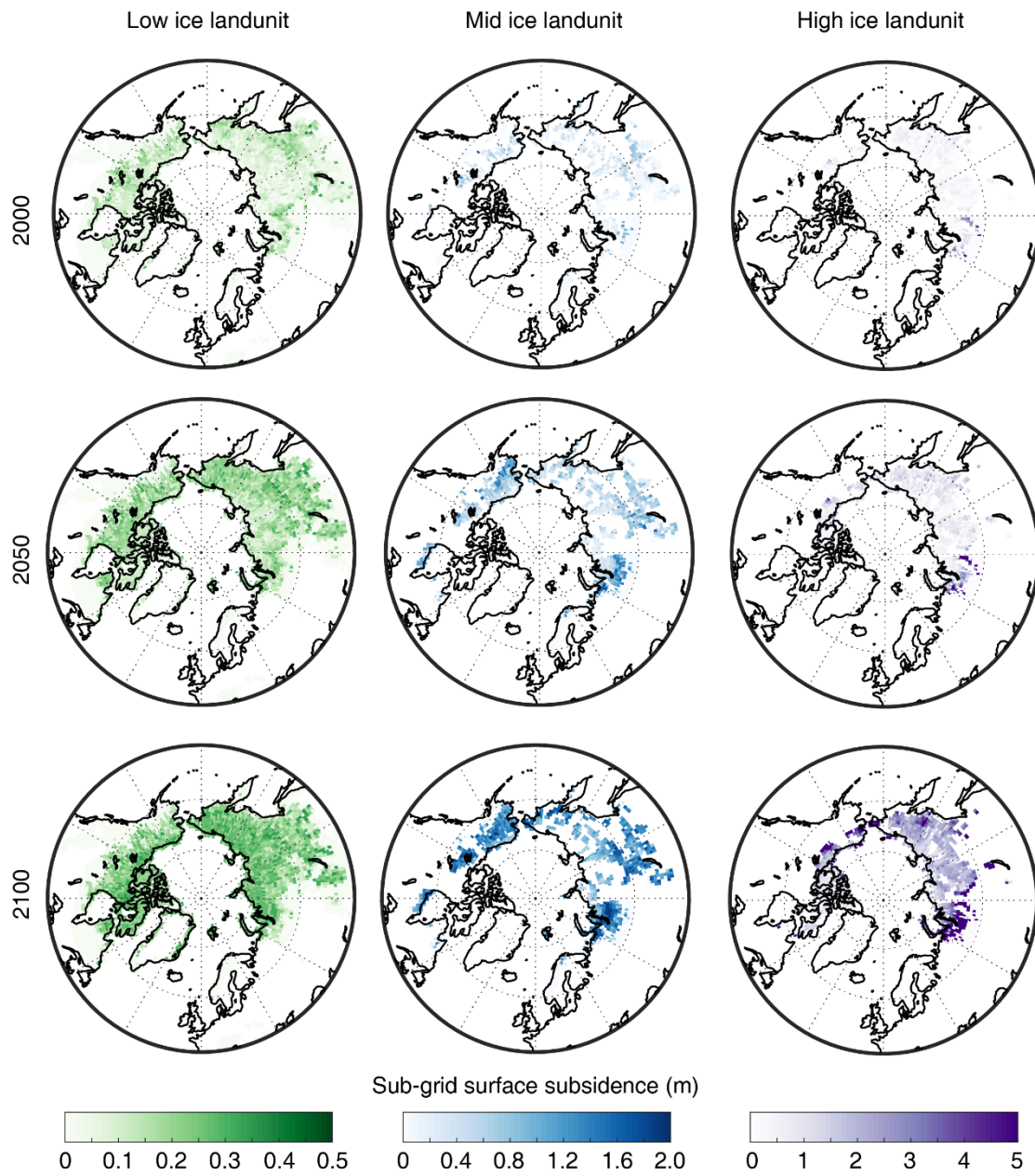
Figure 4. Annual freeze-thaw state for the three terraces for the triple-landunit case, as well as for the average ice single-landunit case.



752

753 **Figure 5. Grid-mean excess ice melt since 1900 for the single-point cases over the Lena river delta**  
 754 **with and without the sub-grid excess ice initialization.**

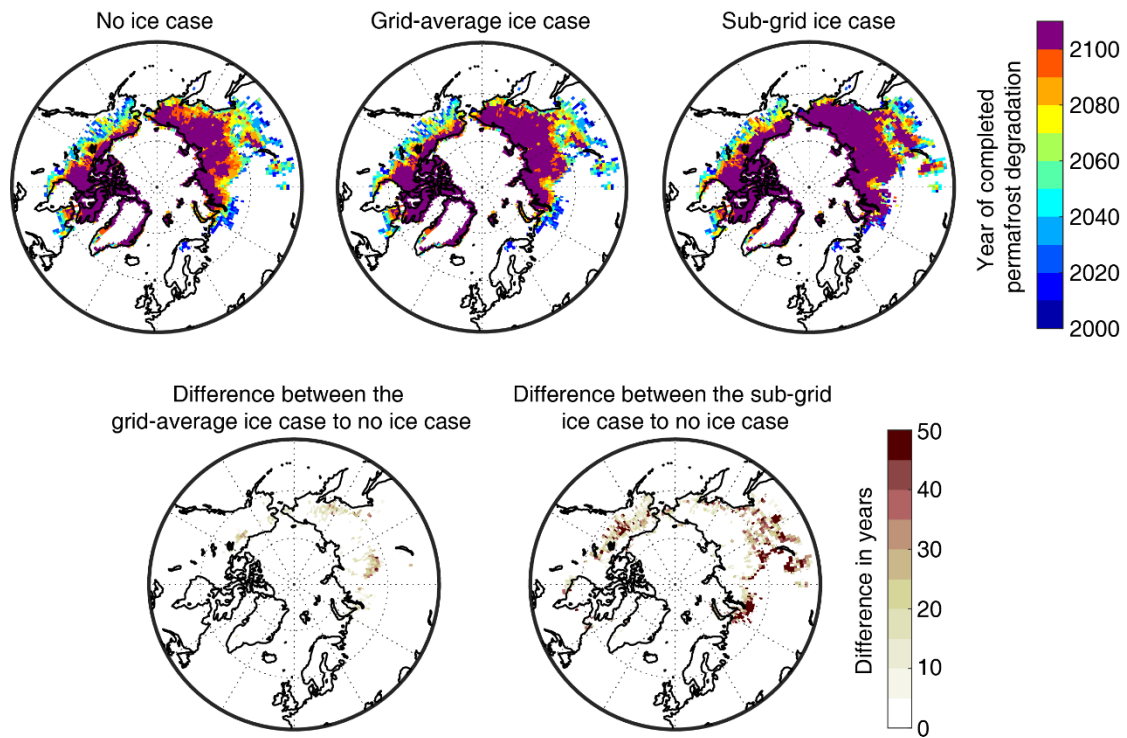
755



756

757 **Figure 6. Maps showing sub-grid surface subsidence (m) in 2000, 2050, 2100 in the low, mid, and**  
 758 **high excess ice landunits in the sub-grid ice case.**

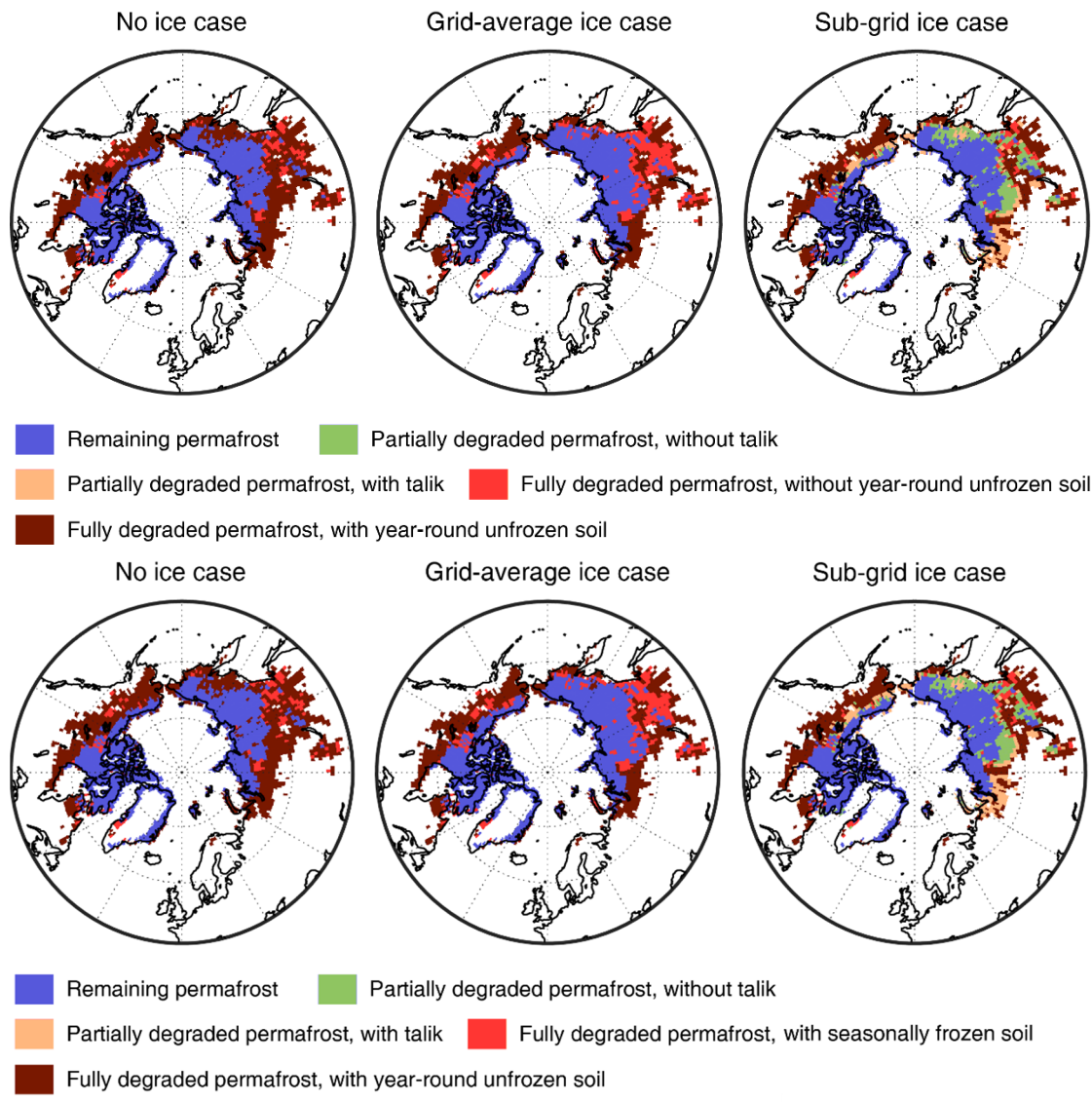
759



760

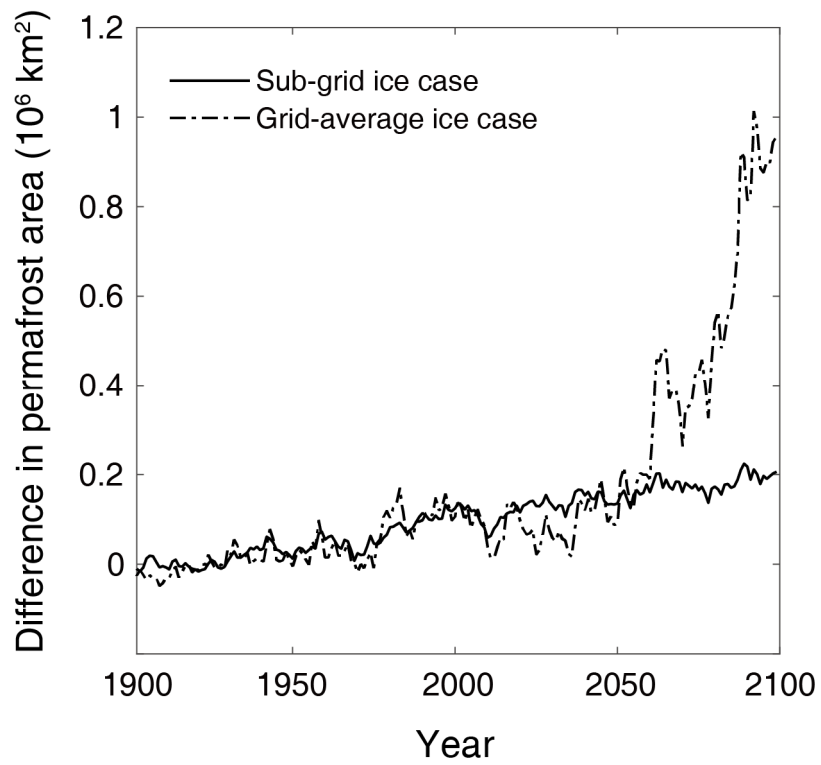
761 **Figure 7. Maps showing the year of completed permafrost degradation (upper set of three maps),**  
 762 **as well as the differences between cases (lower set of two maps). The purple color indicates the**  
 763 **existence of permafrost in these grid cells by 2100. The difference in years is provided only for grid**  
 764 **cell with completed permafrost degradation before 2100.**

765



768 **Figure 8. Maps of different stages of permafrost degradation diagnosed from the model output by**  
 769 **the year 2100. “Year-round unfrozen soil” in the fully degraded permafrost region is defined as the**  
 770 **part of degraded permafrost in which the soil temperature never decrease below 0 °C in any time**  
 771 **of year, which is in the same manner as talik in the permafrost area.**

772



773

774 **Figure 9. Difference in modeled permafrost area versus time between the sub-grid ice case and no**  
775 **ice case, as well as between the grid-average ice case and no ice case.**

776